Dalton Transactions

ROYAL SOCIETY OF CHEMISTRY

PAPER

View Article Online
View Journal | View Issue



Cite this: *Dalton Trans.*, 2025, **54**, 605

# Ru(II)-diphosphine/N,S-mercapto complexes and their anti-melanoma properties†

Nádija N. P. da Silva,[a] Marcos V. Palmeira-Mello,[a] Nathália O. Acésio,[b] Carlos A. F. Moraes,[a] João Honorato,[c] Eduardo E. Castellano,[c] Denise C. Tavares,[b] Katia M. Oliveira *[d] and Alzir A. Batista *[a]

We have synthesized and characterized a novel series of ruthenium complexes with formulas [RuCl(N–S)(dppm)$_2$]PF$_6$ (**Ru1**), [Ru(N–S)(dppm)$_2$]PF$_6$ (**Ru2**), [Ru(N–S)(dppe)$_2$]PF$_6$ (**Ru3**), [Ru(N–S)(dppen)$_2$]PF$_6$ (**Ru4**), [Ru(N–S)(bpy)$_2$]PF$_6$ (**Ru5**). In these formulas, N–S or S represents H2mq (2-mercapto-4(3*H*)-quinazoline); dppe (1,2′-bis(diphenylphosphine)ethane), dppm (1,1′-bis(diphenylphosphine)methane), or dppen (1,2′-bis(diphenylphosphine)ethene); and bpy refers to 2,2′-bipyridine. We have also compared the cytotoxicity of cisplatin with these ruthenium complexes to murine melanoma cells (B16-F10), human melanoma cells (A-375), and the non-tumoral human keratinocyte cell line (HaCat). All the ruthenium complexes inhibited melanoma cell growth in a dose-dependent manner. [Ru(2mq)(dppen)$_2$]PF$_6$ was four times more active toward A-375 cells than toward HaCat cells, inhibited colony formation in HaCat and A-375 cells (with a more pronounced effect on A-375 cells), altered A-375 cell morphology, and inhibited cell migration at 0.2 and 0.4 μM. In addition, we investigated how these ruthenium complexes interact with biomolecules such as DNA and Human Serum Albumin (HSA). All the ruthenium complexes interacted weakly with DNA, possibly through the grooves. Based on fluorescence assays, the ruthenium complexes interacted moderately with HSA. In light of these results, ruthenium complexes bearing phosphine and H2mq display promising cytotoxic properties against melanoma.

Received 9th September 2024,
Accepted 11th November 2024

DOI: 10.1039/d4dt02575j

rsc.li/dalton

## Introduction

Cancer, one of the most serious public health problems and a leading cause of death worldwide, is marked by cells that proliferate rapidly and uncontrollably and which infiltrate various tissues and organs. Among the diverse types of cancer, melanoma stands out: it increases at a higher rate than other forms of cancer.[1] Melanoma emerges from mutations in genes that regulate the growth and viability of melanocytes, which are cells that produce melanin and thus offer protection against harmful ultraviolet radiation (UV) and contribute to skin pigmentation. Cutaneous melanoma is the most prevalent form, but melanoma also manifests in tissues like mucous membranes, uveal tract, and leptomeninges.[2,3]

In its early stages, melanoma can be effectively treated with surgery, and the survival rate is high. However, diagnosing melanoma late, as in the case of advanced or metastatic melanoma, restricts treatment options.[2] Therefore, developing methodologies to treat melanoma more effectively while producing fewer or no side effects is crucial, especially when it comes to the advanced stages of the disease.[4]

In clinical practice, chemotherapy based on metal complexes has stood out since cisplatin (*cis*-[PtCl$_2$(NH$_3$)$_2$], *cis*-diamminedichloroplatinum(II)) was discovered and approved by

[a]*Departament of Chemistry, Federal University of São Carlos – UFSCar, CEP 13565-905, São Carlos, SP, Brazil. E-mail: daab@ufscar.br*
[b]*University of Franca – UNIFRAN, CEP 14404-600, Franca, SP, Brazil*
[c]*Physics Institute of São Carlos, University of São Paulo – USP, CEP 13560-970, São Carlos, SP, Brazil*
[d]*Institute of Chemistry, University of Brasília – UnB, CEP 70910-900, Brasília, DF, Brazil. E-mail: katia.oliveira@unb.br*

† Electronic supplementary information (ESI) available: Fig. S1 (infrared spectra of the **Ru1–Ru5** complexes and H2mq ligand); Fig. S2 (cyclic voltammogram of the **Ru1–Ru5** complexes); Fig. S3 and S4 (UV-vis spectra of the **Ru1–Ru5** complexes); Fig. S5–S8 ($^{31}$P{$^1$H} NMR spectra of the **Ru1–Ru5** complexes); Fig. S9–S28 ($^1$H, COSY ($^1$H–$^1$H), $^{13}$C{$^1$H}, HSQC ($^1$H–$^{13}$C), and HMBC ($^1$H–$^{13}$C) NMR spectra of the **Ru1–Ru5** complexes); Fig. S29–S35 ($^{31}$P{$^1$H} NMR spectra of the **Ru1–Ru5** complexes over time in acetone, DMSO, and culture medium); Fig. S36 (UV-vis spectra of **Ru5** complex over time in DMSO/culture medium); Fig. S37 (circular dichroism spectra of CT-DNA in absence and presence of **Ru3–Ru5** complexes); Fig. S38 (fluorescence spectra of CT-DNA-Hoechst and **Ru3–Ru5** complexes); Fig. S39–S41 (fluorescence spectra of HSA in absence and presence of **Ru3–Ru5** complexes); Table S1 (values of coupling constant $^2J_{P-P}$ of **Ru1–Ru4** complexes of $^{31}$P{$^1$H} NMR spectra); Tables S2 and S3 (crystal data and structure refinement for **Ru1**, **Ru2**, **Ru3** and **Ru5** complexes); Table S4 (thermodynamic parameters of the **Ru2–Ru5** complexes with HSA). CCDC 2355448 (**Ru1**), 2355449 (**Ru2**) and 2355450 (**Ru5**). For ESI and crystallographic data in CIF or other electronic format see DOI: https://doi.org/10.1039/d4dt02575j

the FDA (Food and Drug Administration).[5] This drug displays broad cytotoxic action and has proven effective for treating lung, head, ovarian, testicular, and esophageal cancer, for instance. Unfortunately, many issues related to side effects and acquired resistance have been reported after continuous use of this chemotherapy.[6–8]

To mitigate the undesired effects of cisplatin, researchers have developed new platinum-based compounds with different structures, where mono- or bidentate ligands replace amine ligands to modulate electronic, steric, and basicity effects. Examples of these compounds include carboplatin, oxaliplatin, and nedaplatin, among others.[9] Although some side effects have been reduced, others have persisted during chemotherapeutic treatment. Consequently, the scientific community has been exploring alternative metal centers in an endeavor to develop complexes that target tumor cells more effectively and selectively.[10,11]

Ruthenium has been extensively researched in this context, and ruthenium complexes have been shown to exhibit promising cytotoxic and antitumor activities.[12] Among the ruthenium complexes with potential chemotherapeutic action,[13–15] the BOLD-100 or KP-1339 (*trans*-[tetrachlorobis(1*H*-indazole)ruthenate(III)]) complex, developed by Keppler and colleagues, is noteworthy. This compound induces DNA damage, cell cycle arrest, and apoptosis and is now undergoing clinical trials.[10] In this regard, our research group has developed novel ruthenium complexes with different phosphine co-ligands to enhance the cytotoxic activity of the final complexes by taking advantage of the synergism that might occur between the metal center and the ligands in the coordination sphere.[16–18]

N,S-Mercapto comprises a group of molecules that can act as ligands and which have attracted our attention. When these ligands coordinate to ruthenium, notably cytotoxic complexes arise, particularly complexes featuring phosphine as co-ligands.[18–20]

In this study, we aimed to synthesize novel ruthenium complexes containing 2-mercapto-4(3*H*)-quinazoline as ligand and different phosphines as co-ligands. Our goal was to establish a possible structure–activity relationship and to explore how changing the substituents in the phosphine groups affects the cytotoxicity of the ruthenium complexes toward melanoma cell lines. Additionally, we have investigated how the ruthenium complexes interact with biomolecules such as CT-DNA and human serum albumin (HSA).

# Experimental section

### General methods and materials

All the syntheses were conducted under argon atmosphere. $RuCl_3{\cdot}nH_2O$, H2mq (2-mercapto-4(3*H*)-quinazoline), dppe [1,2′-bis(diphenylphosphine)ethane], dppm [1,1′-bis(diphenylphosphine)methane], dppen [1,2′-bis(diphenylphosphine) ethene], bipy (2,2′-bipyridine), calf-thymus DNA (CT-DNA), human serum albumin (HSA), and 3-(4,5-dimethylthiazol-2-yl)-2,5-diphenyltetrazolium bromide (MTT) were purchased from either Merck or Sigma Aldrich and were used as received. The *cis*-$[RuCl_2(dppm)_2]$, *cis*-$[RuCl_2(dppe)_2]$, *cis*-$[RuCl_2(dppen)_2]$, and *cis*-$[RuCl_2(bipy)_2]$ precursor complexes were synthesized by using a well-established procedure.[21–24]

The IR spectra of the ruthenium complexes were acquired from 4000 to 400 $cm^{-1}$ on a Bomem–Michelson 102 Fourier transform infrared spectrometer; KBr pellets were used. Molar conductivity was measured on a Meter Lab CDM2300 instrument; $1 \times 10^{-3}$ M DMSO or dichloromethane solutions of the ruthenium complexes were employed. Elemental analyses were carried out on a Fisions CHNS analyzer model EA 1108 at the Central Analytical Laboratory of the Department of Chemistry at the Federal University of São Carlos, São Carlos, São Paulo, Brazil. UV-visible absorption spectra were recorded from 250 to 700 nm on a Hewlett-Packard 8452A diode array spectrophotometer; DMSO or dichloromethane solutions of the ruthenium complexes were placed in quartz cuvettes of 1 cm optical path length. Cyclic voltammetry assays were performed on an EGeG Princeton Applied Research Model 273A Potentiostat/Galvanostat by using an electrochemical cell with a three-electrode system, namely Ag/AgCl as the reference electrode and two platinum plates as the auxiliary and working electrodes, immersed in 0.1 mol $L^{-1}$ tetrabutylammonium perchlorate (TBAP, Fluka Chemica) solution in dichloromethane. $^{31}P\{^1H\}$, $^1H$, COSY ($^1H$–$^1H$), $^{13}C\{^1H\}$, HSQC ($^1H$–$^{13}C$), and HMBC ($^1H$–$^{13}C$) NMR spectra were recorded on a 9.4 T Bruker Avance III 400 MHz spectrometer.

### $[RuCl(H2mq)(dppm)_2]PF_6$ (Ru1)

To obtain **Ru1**, 0.018 g (0.10 mmol) of H2mq was added to a Schlenk flask containing a deaerated methanol/dichloromethane mixture (5 : 1). The system was stirred and refluxed until the ligand was completely dissolved. Then, 0.10 g (0.10 mmol) of *cis*-$[RuCl_2(dppm)_2]$ and 0.019 g (0.10 mmol) of $KPF_6$ were added. The system was kept under identical conditions for an additional hour, and then the volume was reduced to around 2 mL. Ethyl ether was introduced to induce precipitation of a yellow powder, which was filtered, rinsed with distilled water and ethyl ether, and dried under vacuum. Yield: (0.080 mmol; 0.098 g) 76%. Anal. calcd for $C_{58}H_{50}ClF_6N_2OP_5SRu$: C, 56.71; H, 4.10; N, 2.28; S, 2.61. Found: C, 56.86; H, 3.96; N, 2.44; S, 3.03. ESI-MS calcd for $[Ru(2mq)(dppm)_2]^+$ ($[M]^+$): *m*/*z* 1047.1560. Found: *m*/*z* 1047.1554. Selected IR (KBr, $\nu$, $cm^{-1}$) 3056 ($\nu C_{sp^2}$–H); 1625 ($\nu$C=N); 1560 ($\nu$C=C + $\nu$C=N); 1261 ($\nu$C–S); 1906 ($\nu$P–C); 836 ($\nu PF_6^-$); 726 ($\delta$C–H (ring)); 560 ($\delta PF_6^-$); 482 ($\nu$Ru–S); 414 ($\nu$Ru–N). $^{31}P\{^1H\}$ NMR (162 MHz, $D_2O$) $\delta$ −1.73 (1P, dt, $J$ = 41.7, 28.5 Hz); −3.82 (1P, dt, $J$ = 37.9, 27.7 Hz); −22.17 (1P, ddd, $J$ = 324.0, 41.8, 27.7 Hz); −23.68 to −26.55 (1P, m); −143.04 (1P, hept, $PF_6^-$). $^1H$ NMR (400 MHz, acetone-$d_6$): $\delta$ 13.54 (1H, s, H2mq); 12.23 (1H, s, H2mq) 8.34–6.80 (44H, m, aromatics of dppm and H2mq); 5.7–5.0 (4H, m, dppm). $^{13}C$ NMR (101 MHz, acetone-$d_6$, 298 K, ppm) $\delta$ 173.64 (1C, s, H2mq (C=S)); 157.61 (1C, s, H2mq (C=O)); 138.95–125.92 (52C, m, aromatics of dppm and H2mq); 117.40 (1C, s, dppm); 116.84 (1C, s, dppm).

### $[Ru(2mq)(dppm)_2]PF_6$ (Ru2)

In a Schlenk flask containing 20 mL of deaerated methanol, 0.022 g (0.12 mmol) of H2mq and 0.011 g (0.13 mmol) of $NaHCO_3$ were added. The system was stirred and refluxed for 1 h, and then 0.10 g (0.10 mmol) of *cis*-$[RuCl_2(dppm)_2]$ and 0.023 g (0.12 mmol) of $KPF_6$ were added. The system was stirred and refluxed for other 24 h. After that, the volume was reduced to approximately 2 mL, and distilled water was added to induce precipitation of a yellow solid, which was filtered, washed with distilled water and ethyl ether, and dried under vacuum. Yield: (0.083 mmol; 0.100 g) 79%. Anal. calcd for $C_{58}H_{49}F_6N_2OP_5SRu$: C, 58.44; H, 4.14; N, 2.35; S, 2.69. Found: C, 58.23; H, 4.23; N, 2.32; S, 2.46. ESI-MS calcd for $[Ru(2mq)(dppm)_2]^+$ ($[M]^+$): *m*/*z* 1047.1554. Found: *m*/*z* 1047.1582. Selected IR (KBr, $\nu$, $cm^{-1}$): 3061 ($\nu C_{sp^2}$–H); 1613 ($\nu$C═N); 1436 ($\nu$C═C + $\nu$C═N); 1244 ($\nu$C–S); 1906 ($\nu$P–C); 839 ($\nu PF_6^-$); 732 ($\delta$C–H (ring)); 561 ($\delta PF_6^-$); 484 ($\nu$Ru–S); 418 ($\nu$Ru–N). $^{31}P\{^1H\}$ NMR (162 MHz, $D_2O$): $\delta$ 0.92 to −0.51 (1P, m); −8.07 to −9.23 (1P, m); −11.68 (1P, ddd, $J$ = 312.9, 42.2, 26.8 Hz); −22.33 (1P, ddd, $J$ = 67.3, 40.2, 27.8 Hz); −143.64 (1P, hept, $PF_6^-$). $^1H$ NMR (400 MHz, DMSO-$d_6$): $\delta$ 8.19–6.56 (54H, m, aromatics of dppm and H2mq); 5.60–4.60 (4H, m, H2mq). $^{13}C$ NMR (101 MHz, DMSO-$d_6$, 298 K, ppm) $\delta$ 178.12 (1C, s, H2mq (C–S)); 165.86 (1C, s, H2mq (C═O)); 159.76 (1C, s, H2mq); 148.48 (1C, s, H2mq); 138.20–116.76 (52C, m, aromatics of dppm and H2mq).

### $[Ru(2mq)(dppe)_2]PF_6$ (Ru3)

**Ru3** was synthesized according to the procedure reported in the literature.[19] Yield: (0.077 mmol; 0.094 g) 75%. Anal. calcd for $C_{60}H_{53}F_6N_2OP_5SRu$: C, 59.07; H, 4.38; N, 2.30; S, 2.63. Found: C, 58.98; H, 4.46; N, 2.49; S, 2.82.

### $[Ru(2mq)(dppen)_2]PF_6$ (Ru4)

To obtain **Ru4**, 0.014 g (0.14 mmol) of H2mq and 32 μL of triethylamine were added to a Schlenk flask containing 30 mL of a deaerated methanol/dichloromethane mixture (1 : 1). After 10 min, 0.10 g (0.10 mmol) of *cis*-$[RuCl_2(dppen)_2]$ and 0.028 g (0.15 mmol) of $KPF_6$ were added. The system was stirred and refluxed for 12 h, and then the volume was reduced to approximately 2 mL. Distilled water was incorporated to induce precipitation of a yellow powder, which was filtered, washed with distilled water and ethyl ether, and dried under vacuum. Yield: (0.078 mmol; 0.095 g) 76%. Anal. calcd for $C_{60}H_{49}F_6N_2OP_5SRu$: C, 59.26; H, 4.06; N, 2.30; S, 2.64. Found: C, 59.38; H, 4.15; N, 2.72; S, 2.69. ESI-MS calcd for $[Ru(2mq)(dppen)_2]^+$ ($[M]^+$): *m*/*z* 1071.1554. Found: *m*/*z* 1071.158. Selected IR (KBr, $\nu$, $cm^{-1}$): 3056 ($\nu C_{sp^2}$–H); 1625 ($\nu$C═N); 1560 ($\nu$C═C + $\nu$C═N); 1261 ($\nu$C–S); 1906 ($\nu$P–C); 836 ($\nu PF_6^-$); 726 ($\delta$C–H (ring)); 560 ($\delta PF_6^-$); 482 ($\nu$Ru–S); 414 ($\nu$Ru–N). $^{31}P\{^1H\}$ NMR (162 MHz, $D_2O$) $\delta$ 69.08–66.87 (1P, m); 59.57 (1P, m); 56.73 (1P, m); 53.16–51.73 (1P, m); −143.64 (1P, hept, $PF_6^-$). $^1H$ NMR (400 MHz, DMSO-$d_6$): $\delta$ 8.95–6.54 (44H, m, aromatics of dppen and H2mq); 6.22–5.71 (4H, m, dppen). $^{13}C$ NMR (101 MHz, DMSO-$d_6$, 298 K, ppm) $\delta$ 171.51 (1C, s, H2mq (C–S)); 159.02 (1C, s, H2mq); 144.88 (1C, s, H2mq (C═O)); 138.40 (1C, s, H2mq); 134.60–127.11 (52C, m, aromatics of dppen and H2mq); 122.88 (4C, s, dppen).

### $[Ru(2mq)(bipy)_2]PF_6$ (Ru5)

To synthesize **Ru5**, 0.044 g (0.24 mmol) of H2mq was added to a Schlenk flask containing 32 mL of an ethanol/water mixture (1 : 1). The system was stirred and refluxed until the ligand was completely dissolved. Subsequently, 0.10 g (0.20 mmol) of *cis*-$[RuCl_2(bipy)_2]$ and 0.114 g (0.61 mmol) of $KPF_6$ were added. The system was maintained under the same conditions until precipitation of a red solid, which was separated by filtration, washed with 3 mL of distilled water and 3 mL of ethyl ether, and dried under vacuum. Yield: (0.184 mmol; 0.135 g) 89%. Anal. calcd for $C_{28}H_{21}F_6N_6OPSRu$: C, 45.72; H, 2.88; N, 11.42; S, 4.36. Found: C, 45.83; H, 3.03; N, 11.34; S, 4.52. ESI-MS calcd for $[Ru(2mq)(bipy)_2]^+$ ($[M]^+$): *m*/*z* 591.0536. Found: *m*/*z* 591.0553. Selected IR (KBr, $\nu$, $cm^{-1}$): 3072 ($\nu C_{sp^2}$–H); 1603 ($\nu$C═N); 1523 ($\nu$C═C + $\nu$C═N); 1245 ($\nu$C–S); 844 ($\nu PF_6^-$); 729 ($\delta$C–H (ring)); 557 ($\delta PF_6^-$); 479 ($\nu$Ru–S); 423 ($\nu$Ru–N). $^1H$ NMR (400 MHz, DMSO-$d_6$): $\delta$ 12.76 (1NH, s, H2mq); 9.73–7.16 (19H, m, aromatics of bipy and H2mq); 5.34 (1H, d, H2mq). $^{13}C$ NMR (101 MHz, DMSO-$d_6$, 298 K, ppm) $\delta$ 174.74 (1C, s, H2mq (C–S)); 160.63 (1C, s, H2mq); (1C, s, H2mq (C═O)); 159.22–118.16 (26C, m, aromatics of bipy and H2mq).

### X-ray crystallography

**Ru1**, **Ru2**, **Ru3**, and **Ru5** monocrystals were obtained by slow evaporation in acetone, dichloromethane/methanol, acetone/methanol, and methanol, respectively. The X-ray single-crystal diffraction measurements were carried out at the Institute of Physics, University of São Paulo in São Carlos, São Paulo, Brazil. Data were collected on a Rigaku XtaLAB Mini (ROW) or XtaLAB Synergy Dualflex HyPix diffractometer, with MoKα ($\lambda$ = 0.71073). The crystal structures were determined through direct methods by using the SHELXL[25] program and refined by the least-squares method with the aid of the SHELXL program. The crystallographic data and structures of **Ru1**, **Ru2**, **Ru3**, and **Ru5** were generated with the OLEX[26] program.

### Studies on the interaction with DNA

**CT-DNA preparation.** CT-DNA (*Calf Thymus* deoxyribonucleic acid sodium salt, Sigma-Aldrich) was prepared in 10 mL of Tris-HCl buffer (0.5 mM Tris-base, 4.5 mM Tris-HCl, and 50 mM NaCl; pH 7.4). The CT-DNA concentration was determined by UV-Vis, by using the absorbance and molar absorptivity of DNA at 260 nm ($\varepsilon$ = 6600 $cm^{-1}$ $mol^{-1}$ L) and the optical path length ($b$ = 1 cm), according to the Lambert–Beer law: $A_{260} = \varepsilon \times b \times c$.

**Viscosity analysis.** The assay was conducted by preparing 80 μM CT-DNA solutions in Tris-HCl buffer (pH 7.4) containing 40% DMSO in both the presence and absence of a certain concentration of one of the ruthenium complexes. Measurements were carried out with an Ostwald viscometer in a water thermostatic bath at 25 °C. The flow time of each solution was measured in quintuplicate; a digital stopwatch was

employed. The viscosity results were derived from the flow times of the CT-DNA solutions and graphed as $(\eta/\eta_0)^{1/3}$ *versus* [ruthenium complex]/[CT-DNA], where $\eta$ and $\eta_0$ represent the relative DNA viscosity in the presence and absence of a ruthenium complex, respectively. For comparison purposes, thiazole orange, known for its capacity to intercalate with DNA, and cisplatin, which can covalently bind to DNA, were employed.

**Hoechst 33258 displacement assay.** Initially, Hoechst and CT-DNA solutions were prepared in Tris-HCl buffer (pH 7.4) at 5 and 100 μM, respectively. By using this solution, mixtures containing various concentrations of one of the ruthenium complexes (from 5 to 40 μM) were prepared. In each solution, the DMSO percentage was kept at 10%. Aliquots of 200 μL of this mixture (Hoechst + CT-DNA + ruthenium complex) were added to 96-well opaque plates, and fluorescence emission spectra were acquired under excitation at 343 nm on a Synergy/H1-Biotek fluorimeter equipped with a monochromator.

**Circular dichroism.** CT-DNA (100 μM) and **Ru2–Ru5** (varying concentrations) solutions were prepared in Tris-HCl buffer (pH 7.4) to achieve [ruthenium complex]/[CT-DNA] molar ratios ranging from 0.06 to 0.25. The DMSO percentage was maintained at 10%. Additionally, solutions containing only one of the ruthenium complexes and only CT-DNA were prepared as blanks and controls, respectively. The samples were incubated at 310 K for 18 h. Spectra were recorded between 240 and 400 nm at 200 nm $min^{-1}$ by using a JASCO J720 spectropolarimeter and five accumulations per measurement, at 298 K. The nitrogen flow was kept constant throughout the measurements.

**Agarose gel electrophoresis.** Samples containing pBR322 plasmid DNA (30 μM) and one of the ruthenium complexes at a certain concentration (7.5 or 15 μM) in Tris-HCl buffer containing 10% of DMSO were incubated at 310 K for 18 h. After incubation, 10 μL of each sample was subjected to electrophoresis within a 1% agarose gel immersed in TAE buffer (0.45 μM Tris-HCl, 0.45 μM acetic acid, and 10 mM EDTA; pH 7.4). Analyses were carried out in a Bio-Rad horizontal tank connected to a Consort EV231 variable-potential power supply. Subsequently, the gels were stained in a 2 μg $mL^{-1}$.

### Interaction with human serum albumin (HSA)

Interactions between **Ru2–Ru5** and HSA (from Sigma Aldrich) were studied by measuring HSA fluorescence suppression in the presence of different concentrations of a ruthenium complex. To investigate the type of interaction, the experiment was conducted at 298, 303, or 310 K. The HSA solution was prepared by solubilization in Tris-HCl buffer (pH 7.4), and the concentration was determined by UV-vis spectroscopy on the basis of the molar absorptivity at 280 nm ($\varepsilon$ = 36 500 $cm^{-1}$ $mol^{-1}$ L).

In 1000 μL microtubes, increasing aliquots (5–40 μL) of one of the ruthenium complexes in DMSO were added, and the volume was adjusted to 50 μL (5%) with DMSO. To the microtubes, 950 μL of the stock HSA solution was added to reach a final volume of 1000 μL. HSA and DMSO solutions in the absence of a ruthenium complex were used as controls. Aliquots of 200 μL were taken from each microtube and transferred to a 96-well opaque plate; measurements were performed in triplicate. Fluorescence emission was measured from 260 to 500 nm under excitation at 270 nm on a Synergy/H1-Biotek fluorometer equipped with a monochromator.

The fluorescence quenching process was quantitatively analyzed by using the Stern–Volmer equation:[27]

$$F_0/F = 1 + k_q\tau_0[Q] = 1 + K_{SV}[Q] \quad (1)$$

where $F_0$ and $F$ represent the fluorescence intensity in the absence and presence of the quencher (**Ru2–Ru5**), respectively; [Q] denotes the quencher concentration; $K_{SV}$ corresponds to the Stern–Volmer quenching constant; $k_q$ stands for the biomolecular quenching constant; and $\tau_0$ represents the average lifetime of HSA without the quencher ($\sim 10^{-8}$ s).[27]

To determine the binding constant ($K_b$) and the number of binding sites ($n$), eqn (2) was employed:

$$\log[(F_0 - F)/F] = \log K_b + n \log[Q] \quad (2)$$

The thermodynamic parameters ($\Delta H°$, $\Delta S°$, and $\Delta G°$) were derived from eqn (3) and (4):[28]

$$\ln(K_{b1}/K_{b2}) = (1/T_1 - 1/T_2) \times \Delta H/R \quad (3)$$

where $K_1$ and $K_2$ are the binding constants at temperatures $T_1$ and $T_2$, respectively; and $R$ is the constant of the ideal gases.

$$\Delta G° = -RT \ln K_b = \Delta H° - T\Delta S° \quad (4)$$

### General cell culture

The cell lines employed in this study included the human melanoma (A-375) and murine melanoma (B16-F10) cell lines and a non-tumoral human keratinocyte cell line (HaCat). A-375 and B16-F10 were provided by S. S. Maria-Engler, University of São Paulo, São Paulo, Brazil and HaCat cells was provided by P. F. Oliveira, Federal University of Alfenas, Alfenas, Minas Gerais, Brazil. All the cell lines were cultivated in Dulbecco's Modified Eagle Medium Nutrient (DMEM – Sigma Aldrich) supplemented with 10% fetal bovine serum, antibiotics (0.001 mg $mL^{-1}$ streptomycin and 0.005 mg $mL^{-1}$ penicillin – Sigma Aldrich), and 2.38 mg $mL^{-1}$ Hepes (Sigma Aldrich). The cells were cultured as monolayers in 25-$cm^2$ disposable flasks at 37 °C under 5% $CO_2$.

**Cytotoxicity.** The cytotoxicity of **Ru2–Ru5** was determined by using the XTT colorimetric assay (Cell Proliferation Kit II – Roche Diagnostics, Basel, Switzerland); the manufacturer's instructions were followed. This assay suggests that cell viability is proportional to the formation of formazan, which occurs during XTT reduction. The cells were trypsinized for counting and adjusting the cell concentration. Then, they were seeded into 96-well plates ($1 \times 10^4$ cells per well) and incubated in a humidified incubator at 37 °C and under 5% $CO_2$ for 24 h for cell adhesion. Subsequently, one of the ruthenium complexes was added at a certain concentration (from 100 to 0.78 μM), and the plates were maintained in the incubator for 24 h. Cells treated with 1% DMSO were used as controls. After treatment

 

for 24 h, the culture medium was removed, and the cells were washed with 100 μL of PBS (Phosphate Buffered Saline). Then, 75 μL of XTT solubilized in HAM-F10 culture medium without phenol red (Sigma Aldrich) was added to the wells and incubated for 17 h. The absorbance at 450 nm of the wells was recorded by using a microplate reader (ELISA-Asys-UVM 340/microwin 2000). From the absorbance, $IC_{50}$ (concentration required to inhibit cell viability by 50%) was calculated.

**Colony formation assay.** The antiproliferative activity of **Ru4** was investigated by employing the clonogenic efficiency assay, as described by Franken *et al.*[29] For this purpose, HaCat, A-375, or B16-F10 cells were seeded (300 cells per well) in six-well plates and incubated at 37 °C and under 5% $CO_2$ for 2 h. After that, a culture medium containing one of the ruthenium complexes at a certain concentration (from 0.5 to 4 μM), determined based on the cell viability results, was added, and the plates were incubated for 24 h. The culture medium was removed, the wells were washed with PBS, and a fresh culture medium was added. The plates were kept in an incubator at 37 °C and under 5% $CO_2$ for 10 days. After incubation, the culture medium was removed, and colonies were fixed with a methanol/glacial acetic acid/distilled water solution (1 : 1 : 8) and stained with Giemsa (phosphate buffer 1 : 20, pH 7.4) for 20 min The number of colonies was counted by using the Image J software.

**Cell morphology analysis.** To assess how **Ru4** impacts cell morphology, A-375 cells were plated in 24-well plates ($0.6 \times 10^5$ cells per well) and incubated at 37 °C and under 5% $CO_2$ for 24 h to promote adhesion. Subsequently, the cells were exposed to varying **Ru4** concentrations (from 0.625 to 20 μM), and images were taken immediately after treatment and after incubation for 24 h; an inverted microscope equipped with a camera was employed. This experimental procedure was conducted in triplicate.

**Cell migration assay.** The ability of **Ru4** to inhibit cell migration was analyzed by using the *Wound Healing* assay. A-375 cells were seeded ($1.3 \times 10^5$ cell per well) in 24-well plates and maintained in an incubator at 37 °C and under 5% $CO_2$ for 24 h to allow adhesion. Subsequently, with the aid of a sterile pipette tip, a scratch was made on the adherent cell monolayer, and the culture medium containing cellular debris was removed. Culture medium containing 1% FBS and **Ru4** at a certain concentration was added to the wells. Control cells received 1% DMSO. Cell images were captured immediately after treatment and after treatment for 24 h. The distances between the scratch edges were measured by using the ImageJ software, and the percentage of closure was determined as follows: wound healing area (%) = [cell-free area (0 h) − cell-free area (24 h)]/cell-free area (0 h) × 100.

## Results and discussion

### Synthesis and characterization of ruthenium/diphosphine/N,S-mercapto complexes

The reaction of *cis*-$[RuCl_2(dppm)_2]$, *cis*-$[RuCl_2(dppe)_2]$, *cis*-$[RuCl_2(dppen)_2]$, or *cis*-$[RuCl_2(bpy)_2]$ with H2mq (2-mercapto-4(3*H*)-quinazoline) resulted in four novel ruthenium complexes (**Ru1**, **Ru2**, **Ru4**, and **Ru5**), which we properly isolated and characterized (Fig. 1). **Ru3** had previously been synthesized and documented.[19] In this study, we synthesized it specifically to facilitate comparisons between the obtained structures and biological results.

We obtained **Ru1–Ru5** as hexafluorophosphate salts of the 1 : 1 electrolyte type (Fig. 2), confirmed by molar conductance measurements performed in DMSO (55.7–60.50 μS $cm^{-1}$) and dichloromethane (40 μS $cm^{-1}$, for **Ru1**). The elemental analysis data also agreed with the structures proposed for **Ru1–Ru5**.

The reaction between *cis*-$[RuCl_2(dppm)_2]$ and H2mq in a dichloromethane/methanol mixture (5 : 1) gave **Ru1**, which bears H2mq coordinated to ruthenium through the sulfur atom in a monodentate manner. However, when we introduced sodium bicarbonate into the reaction medium, another coordination mode characterized by chelation and negative charge emerged for the ligand, generating **Ru2**. As in the case of **Ru2**, in **Ru3–Ru5**, H2mq coordinated to ruthenium in a bidentate and anionic fashion, through the S and N atoms.

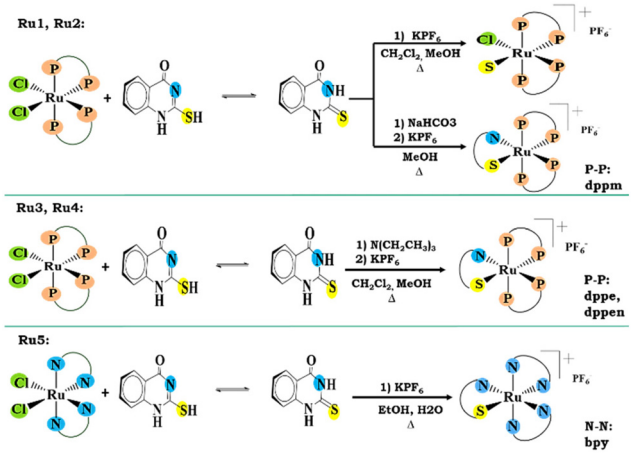


**Fig. 1** Syntheses route used to obtain **Ru1–Ru5** complexes containing 2-mercapto-4(3*H*)-quinazoline as ligand.

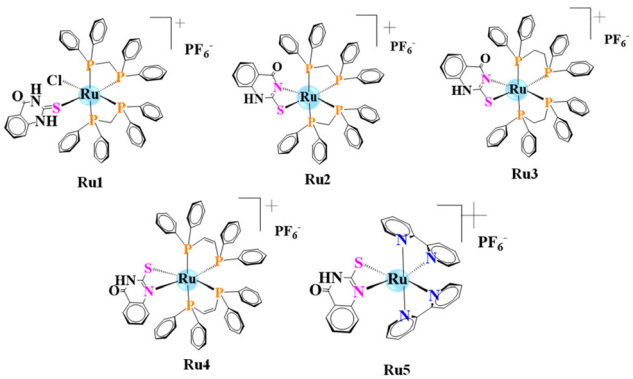


**Fig. 2** Structures of the complexes containing 2-mercapto-4(3*H*)-quinazoline as ligand.

The IR spectra of **Ru1–Ru5** exhibit the same behavior (Fig. S1†). They display bands between 3050 and 3080 $cm^{-1}$, attributed to the stretching of the C–H bond of aromatic rings. The bands between 1630 and 1430 $cm^{-1}$ corresponded to stretching of the $\nu$(C=C) and $\nu$(C=N) bonds of the aromatic rings of the phosphine, bipyridine, and mercapto ligands. Characteristic vibrations assigned to the $\nu$(P–F) and $\delta$(P–F) bonds of $PF_6^-$ appeared between 850 and 550 $cm^{-1}$.[30]

The electrochemical behavior of **Ru1–Ru5** by cyclic voltammetry was investigated. **Ru1–Ru5** behaved similarly, with the $Ru^{II}/Ru^{III}$ oxidation potential ranging from 0.95 to 1.53 V and the $Ru^{III}/Ru^{II}$ reduction potential ranging from 0.48 to 1.06 V (Fig. S2†). **Ru1–Ru5** had higher half-wave potential ($E_{1/2}$) than the respective precursor complexes (Table 1). As expected, when the chloride ligands, which are σ–π donors, with a σ donor and π acceptor ligand, was replaced, the electron density on the metal center decreased due to electron density back-donation from the metal to the ligand. This electrochemically stabilized ruthenium because its oxidation required a higher potential. **Ru1–Ru5** behaved like other phosphine complexes bearing mercapto ligands.[19,31]

The electronic spectra of **Ru1–Ru5** showed an intense absorption in the region of 260 nm for **Ru1–Ru4**, the diphosphine complexes, and 240 nm for **Ru5**, the bipyridine complex. This absorption referred to intraligand transitions (π–π*) of the aromatic rings of the phosphine, bipyridine, and mercapto ligands. The absorptions from 250 to 340 nm in the spectra of **Ru1–Ru4** and from 350 to 520 nm in the spectrum of **Ru5** corresponded to metal-to-ligand charge transfer (MLCT) of the $d\pi_{Ru} \rightarrow 3p\sigma^*d\pi$(phosphine) and $d\pi_{Ru} \rightarrow \pi^*$(bipy, mercapto) type, respectively.

We deconvoluted the electronic spectra of **Ru1–Ru5**. We confirmed the MLCT bands due to $d\pi_{Ru} \rightarrow 3p\sigma^*d\pi$(phosphine) and $d\pi_{Ru} \rightarrow \pi^*$(bipy, mercapto), which were overlapped and resulted in the single MLCT band observed in the electronic spectra. Deconvolution also revealed the d–d transition band, which has a low extinction coefficient and was hidden by the MLCT band (Fig. S3 and S4†).

We characterized **Ru1–Ru5** by $^1$D and $^2$D NMR spectroscopy at different nuclei, including $^{31}P\{^1H\}$, $^{13}C\{^1H\}$, and $^1$H. The $^{31}P\{^1H\}$ NMR spectra of **Ru1–Ru5** exhibited four signals with a double double–double (ddd) pattern, which indicated ABMX spin systems. The phosphorus atom *trans* to nitrogen (N), the most electronegative element among the atoms coordinated to ruthenium, was more deshielded and hence had a greater chemical shift, followed by the phosphorus atom *trans* to sulfur (S). The chemical shifts referring to phosphorus atoms *trans* to phosphorus appeared at lower chemical shifts, and the signals corresponding to these atoms were split into two sets of four lines (Fig. S5–S8†) and had higher coupling constant (Table S1†). The $^{13}C\{^1H\}$ and $^1$H NMR spectra and contour maps are shown in Fig. S9–S26.†

The X-ray crystal structures of **Ru1**, **Ru2**, **Ru3**, and **Ru5** were determined, and Fig. 3 illustrates their ORTEP diagrams. **Ru1**, **Ru2**, **Ru3**, and **Ru5** were hexacoordinated with distorted octahedral geometry: the Ru–S (2.42–2.46 Å) and Ru–P (2.30–2.40 Å) bonds were longer due to the larger atomic radii of phosphorus and sulfur. In comparison, the Ru–N bond (2.13 Å) was shorter. The P–Ru–P and N–Ru–N angles of phosphine and bipyridine, respectively, were larger than the S–Ru–N angles of mercapto ligand (Table 2), as expected.

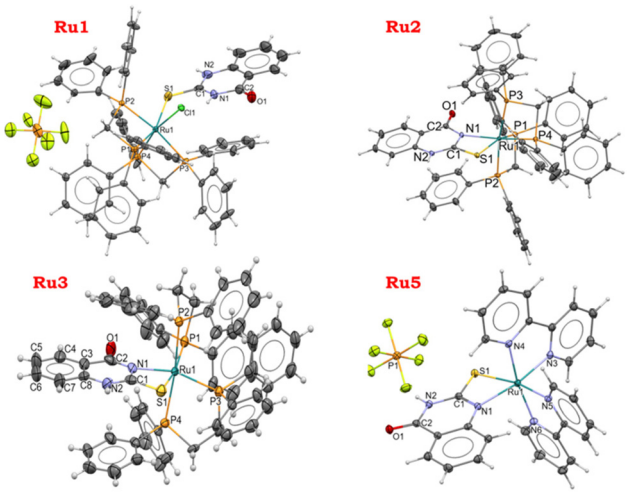


**Fig. 3** Crystal structures of the **Ru1**, **Ru2**, **Ru3**, and **Ru5** complexes ($PF_6^-$ was omitted in **Ru2** and **Ru3**).

**Table 1** Cyclic voltammetry results obtained for the synthesized **Ru1–Ru5** complexes and their respective precursor complexes

| Complex | $E_{pa}$ (V) | $E_{pc}$ (V) | $E_{1/2}$ (V) |
|---|---|---|---|
| **Ru1** | 1.35 | 1.24 | 1.29 |
| **Ru2** | 1.31 | 1.19 | 1.25 |
| *cis*-$[RuCl_2(dppm)_2]$[32] | 1.04 | 0.83 | 0.94 |
| **Ru3** | 1.34 | 1.20 | 1.27 |
| *cis*-$[RuCl_2(dppe)_2]$ | 0.95 | 0.51 | 0.73 |
| **Ru4** | 1.53 | 1.32 | 1.43 |
| *cis*-$[RuCl_2(dppen)_2]$ | 1.06 | 0.97 | 1.02 |
| **Ru5** | 0.95 | 0.83 | 0.87 |
| *cis*-$[RuCl_2(bipy)_2]$ | 0.48 | 0.36 | 0.42 |

**Table 2** $K_{SV}$, $k_q$, $K_b$, parameters for the interaction of the **Ru2–Ru5** complexes with HSA

| Complex | $T$ (K) | $K_{SV}$ ($\times 10^4$ $M^{-1}$) | $K_q$ ($\times 10^{14}$ $M^{-1}$ $s^{-1}$) | $K_b$ ($\times 10^4$ $M^{-1}$) |
|---|---|---|---|---|
| **Ru** | 298 | 5.59 ± 0.36 | 2.79 | 4.93 ± 0.27 |
| | 303 | 5.48 ± 0.49 | 2.74 | 4.84 ± 0.30 |
| | 310 | 5.19 ± 0.55 | 2.59 | 4.49 ± 0.32 |
| **Ru3** | 298 | 5.68 ± 0.20 | 2.84 | 4.57 ± 0.05 |
| | 303 | 5.33 ± 0.03 | 2.67 | 4.44 ± 0.06 |
| | 310 | 5.09 ± 0.01 | 2.54 | 4.38 ± 0.02 |
| **Ru4** | 298 | 4.17 ± 0.23 | 2.09 | 3.66 ± 0.60 |
| | 303 | 3.73 ± 0.11 | 1.87 | 3.37 ± 0.50 |
| | 310 | 3.53 ± 0.15 | 1.77 | 3.26 ± 0.43 |
| **Ru5** | 298 | 3.36 ± 0.11 | 1.68 | 3.19 ± 0.05 |
| | 303 | 3.61 ± 0.08 | 1.80 | 3.38 ± 0.02 |
| | 310 | 3.72 ± 0.11 | 1.86 | 3.52 ± 0.04 |

### Interactions with biomolecules

DNA is a widely exploited target when it comes to developing candidate antitumoral metallodrugs. DNA damage can induce cell death, as seen with cisplatin. Metallodrugs can interact with nucleic acids through non-covalent modes, such as intercalation, insertion, and groove binding, or *via* a covalent mode, including direct binding of the complex to the DNA structure.[33]

In laboratories, several molecular methods are currently used to explore and to classify metallodrug–DNA interactions. Here, we assessed the potential interactions of complexes with CT-DNA by viscosity measurements, competitive assay by fluorescence, circular dichroism, and electrophoresis-based techniques. Variations in DNA viscosity in the presence of a complex provide important information about how a complex interacts with DNA. An intercalating agent, such as thiazole orange, increases the distance between the nitrogenous base pairs, to accommodate the agent, causing the double helix to elongate and DNA viscosity to rise. Covalent interaction elicits the opposite effect—the DNA viscosity decreases because the axial length of the double helix is shortened.[34,35]

Before this study, we investigated whether **Ru1–Ru5** were stable in the solution. First, we recorded the $^{31}P\{^{1}H\}$ NMR spectra of **Ru1**, **Ru2**, and **Ru4** and the $^{1}H$ NMR spectrum of **Ru5**, dissolved in DMSO, at 0, 24, and 48 h. Based on Fig. S29,† only the spectrum of **Ru1**, which contains H2mq as a ligand coordinated in a monodentate manner, changed, and new signals appeared. This indicated that DMSO, a coordinating solvent, replaced H2mq and chloride in the coordination sphere of ruthenium. The spectra of **Ru2–Ru5** remained unaltered during the time of the experiment (Fig. S29–36†).

Similarly, we investigated the stability of **Ru1–Ru5** in a DMSO/culture medium mixture. Except for **Ru1**, all ruthenium complexes remained stable during the evaluated period (Fig. S31–34†). Given that **Ru1** was not stable under the conditions of the biological assays, we did not evaluate its ability to interact with biomolecules or cytotoxic activity.

To characterize how **Ru2–Ru5** interact with DNA, we measured viscosity at constant CT-DNA concentration and varying concentrations of the ruthenium complex, to obtain different [ruthenium complex]/[CT-DNA] molar ratios. Unlike thiazole (an intercalating agent) and cisplatin (which covalently interacts with DNA), adding aliquots of a ruthenium complex to the CT-DNA solution did not modify DNA viscosity significantly (Fig. 4A), indicating that **Ru2–Ru5** established electrostatic or groove interactions. The confidence limits of the viscosity tests can be found in Table S4.†

We also used circular dichroism (CD) to characterize how **Ru2–Ru5** interact with DNA. In the CD spectrum of CT-DNA (Fig. 4A), two bands emerged: the band at 245 nm in the negative region, due to DNA helicity (right-handed twist), and the band at 275 nm in the positive region, due to base stacking. These bands are highly sensitive to interaction between small molecules and DNA. While the CD spectrum of CT-DNA remains unchanged during electrostatic and minor groove binding, intercalation significantly alters both the positive and negative bands.[36–38]

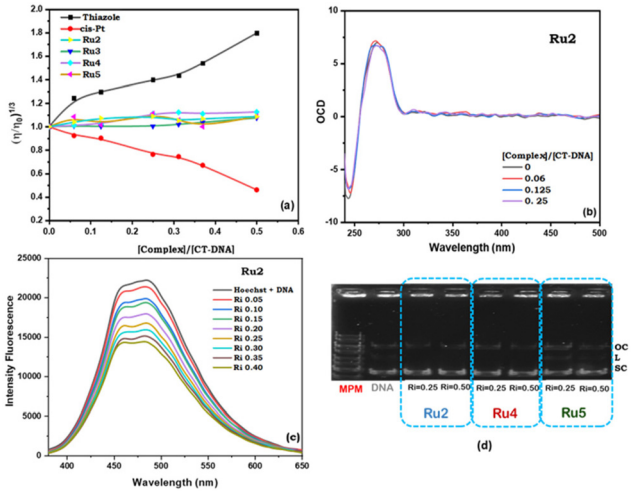


**Fig. 4** (a) CT-DNA (80 μM) viscosity in Tris-HCl buffer (pH 7.4) in the absence and presence of different concentrations of a ruthenium complex (**Ru2–Ru5**), cisplatin, or thiazole orange. (b) Circular dichroism spectra of CT-DNA in the absence and presence of the **Ru2** complex at different [ruthenium complex]/[CT-DNA] molar ratios (Ri) = 0.06–0.25, (c) fluorescence quenching of the CT-DNA-Hoechst complex ($\lambda_{ex}$ = 343 nm) in the absence and presence of different concentrations of the **Ru2** complex, Ri = 0.05–0.40. (d) Electrophoresis mobility shift assays of pBR322 plasmid DNA (30 μM) incubated with different concentrations of the **Ru2** complex.

Fig. 4B shows the CD spectrum of CT-DNA in the presence of **Ru2**. There were no notable alterations in the intensity or position of the DNA bands, which suggested that **Ru2** and DNA interacted weakly, possibly *via* electrostatic or groove interactions. **Ru3**, **Ru4**, and **Ru5** addition to CT-DNA elicited a similar behavior (Fig. S37†).

To confirm whether **Ru2–Ru5** interact with CT-DNA through the grooves, we conducted competition assays by using Hoechst 33258, a fluorescent dye that interacts with DNA through the minor groove, furnishing a DNA-Hoechst complex that emits fluorescence at 460 nm when excited at 340 nm. Increasing **Ru2** concentration decreased the fluorescence intensity of the CT-DNA-Hoechst complex (Fig. 4C), indicating that **Ru2** interacted with DNA *via* the minor groove, displacing Hoechst from this region and suppressing the fluorescence. **Ru3**, **Ru4**, and **Ru5** behaved similarly (Fig. S38†). However, their binding constant ($K_b$) values are higher for the complexes with a similar structure (**Ru2–Ru4**) and lower for the **Ru5** complex (Table S5†).

Furthermore, we employed electrophoretic mobility shift assays in gel to analyze how **Ru2–Ru5** interact with DNA. This assay involves analyzing how DNA moves through a solid phase, such as agarose, under an electrical potential difference. Given that DNA carries a negative charge, it tends to migrate toward the anode. The rate at which DNA moves depends on various factors, including size and conformation. Longer DNA fragments migrate more slowly than shorter ones.[33]

For this analysis, we used plasmid pBR322 DNA, which is primarily in the supercoiled (SC) form and migrates rapidly, in addition to the linear form (LC), which exhibits intermediate migration, and the circular form (OC), which migrates more slowly than SC and LC. By incubating plasmid pBR322 DNA with different concentrations of one of the ruthenium complexes, we observed that the DNA migration rate remained largely unchanged in the presence of **Ru2**, **Ru4**, or **Ru5** compared to the negative control (DNA only) (Fig. 6D). Therefore, these ruthenium complexes did not significantly alter the structure of plasmid pBR322 DNA. Additionally, **Ru3** has been reported to interact with plasmid pBR322 DNA similarly to **Ru2**, **Ru4**, and **Ru5**.[19]

HSA is the most abundant protein in blood and plays a crucial role in carrying substances. Consequently, it can be an important carrier of metallodrugs through the bloodstream. We studied how **Ru2**–**Ru5** interact with HSA, which exhibits intrinsic fluorescence due to amino acid residues, by fluorescence.

We prepared solutions containing HSA at a constant concentration and varying concentrations of one of the ruthenium complexes, to obtain different molar ratios. Fig. 5 presents the fluorescence spectra of HSA in the absence and presence of **Ru2**. The HSA fluorescence became less intense with increasing **Ru2** concentration, indicating that **Ru2** interacted with HSA. We verified the same behavior for **Ru3**–**Ru5** (Fig. S39–S41†).

Quantitative analysis of the fluorescence quenching process allowed us to evaluate whether fluorescence was suppressed through a static or dynamic mechanism. Increasing temperature decreased the quenching constant ($K_{SV}$) of **Ru2**, **Ru3**, and **Ru4**, indicating that fluorescence was suppressed through a static mechanism. In this mechanism, HSA and the quencher (ruthenium complex) form a complex in the ground state, and increasing temperature destabilizes such complex, hence decreasing $K_{SV}$.

For **Ru5**, $K_{SV}$ increased with rising temperature, indicating a dynamic mechanism. In this mechanism, a collision occurs between HSA in the excited state and the quencher (ruthenium complex), which returns to its ground state without emitting fluorescence. Increasing temperature induces more collisions, raising $K_{SV}$. However, $k_q$ obtained for **Ru5** was in the order of $10^{14}$ $M^{-1}$ $s^{-1}$, exceeding the maximum value for a dynamic mechanism ($2.0 \times 10^{10}$ L $mol^{-1}$ $s^{-1}$).[28] Moreover, $k_q$ increased with rising temperature, suggesting that **Ru5** interacted with HSA *via* both the dynamic and static mechanisms.

To evaluate the magnitude of the ruthenium complex–HSA interaction, we calculated the binding constant ($K_b$), which indicated that the interaction was moderate, as judged from the order of magnitude around $10^4$ $M^{-1}$ (Table 2). The number of binding sites was approximately 1, suggesting that the complexes bound to HSA in a 1 : 1 stoichiometry (Table S6†).

We assessed the thermodynamic parameters to investigate the type of interaction between the ruthenium complexes and HSA. $\Delta G$ indicated that the interaction was spontaneous at the studied temperature. Negative $\Delta H$ and positive $\Delta S$, as observed for **Ru2**, **Ru3**, and **Ru4**, indicated electrostatic interactions, whereas positive $\Delta H$ and $\Delta S$, as observed for **Ru5**, indicated hydrophobic interactions[39] (Table S5†).

The complexes that were structurally similar (**Ru2**, **Ru3**, and **Ru4**), with two phosphine ligands, interacted with HSA similarly, showing the same type of mechanism and interaction. Meanwhile, **Ru5**, bearing two bipyridines, exhibited different mechanisms and interactions. This characteristic could be related to the presence of the bipyridine rings, which arranged themselves more orderly around the metal center compared to the bidentate ligands. Such orderly arrangement potentially facilitated interaction of the bipyridine rings with hydrophobic regions of HSA.

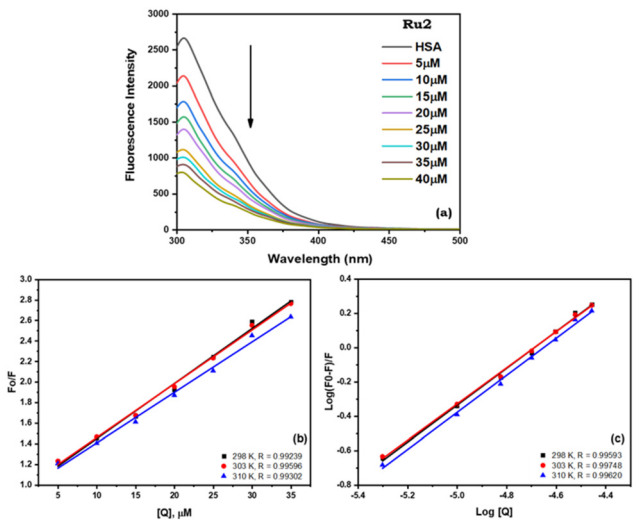


**Fig. 5** (a) Fluorescence spectra of HSA (5 μM, $\lambda_{ex}$ = 270 nm) in the absence and presence of different concentrations of the **Ru2** complex. (b) Stern–Volmer plot and (c) Plot of log[($F_0$ – $F$)/$F$] *vs.* log [Q], at 298, 303, and 310 K.

## Cytotoxicity assays

The cytotoxic activity of **Ru2**–**Ru5** was investigated toward B16-F10 (murine melanoma), A-375 (human melanoma), and HaCat (non-tumoral human keratinocyte) cells. Table 3 lists $IC_{50}$ (concentration of a compound that can inhibit cell viability by 50%) at 24 h and selectivity indexes (SI).

**Ru2**, **Ru3**, and **Ru4**, which contained two phosphine ligands, were cytotoxic toward all the investigated cell lines, whereas **Ru5**, with two bipyridine ligands, was not cytotoxic even at the highest evaluated concentration (200 μM). Therefore, phosphine ligands coordinated to the ruthenium metal center enhanced the cytotoxicity of the ruthenium complexes. Increased cytotoxic activity of ruthenium complexes upon introduction of phosphine ligands has also been observed for other complexes.[40]

We investigated the cytotoxicity of cisplatin, as well, for comparison purposes. **Ru2**, **Ru3**, and **Ru4** showed lower $IC_{50}$ for all the evaluated cell lines. For example, **Ru4** was 4, 2, and 24 times more active than cisplatin toward HaCat, A-375, and B16-F10 cells, respectively. **Ru4** was selective for A-375 cells

 

Table 3 Cytotoxic activity of the **Ru2–Ru5** complexes toward the B16-F10 and A-375 cell lines and the non-tumoral HaCat cell line

| | $IC_{50}$ (μM) – 24 h | | | | |
|---|---|---|---|---|---|
| | HaCat | A-375 | B16-F10 | $IS^1$ | $IS^2$ |
| **Ru2** | 10.70 ± 1.60 | 2.56 ± 0.48 | 20.10 ± 1.40 | 4.18 | 0.53 |
| **Ru3** | 11.73 ± 0.87 | 4.68 ± 0.40 | 3.90 ± 0.30 | 2.50 | 3.00 |
| **Ru4** | 16.32 ± 0.88 | 3.54 ± 0.34 | 6.14 ± 0.21 | 4.61 | 2.66 |
| **Ru5** | >200 | >200 | >200 | — | — |
| Cisplatin | 67.34 ± 1.18 | 6.95 ± 0.03 | 148.11 ± 5.96 | 9.69 | 0.45 |

$IS^1$ = $IC_{50}$ HaCat/$IC_{50}$ A-375 and $IS^2$ = $IC_{50}$ HaCat/$IC_{50}$ B16-F10.

compared to HaCat cells: the SI was 4.61, which made **Ru4** the most selective ruthenium complex studied herein. Thus, we selected **Ru4** to investigate antiproliferative activity by the clonogenic efficiency assay.

The effect of free ligands should also be mentioned. Although their cytotoxicity was not studied here, the literature reveals the absence of anticancer activity for bipy and dppm (an analogue to other phosphine-based ligands) on B16-F10 cancer cells ($IC_{50}$ > 200).[41]

The clonogenic efficiency assay allows one to determine the ability of a cell to proliferate indefinitely and to form colonies comprised of at least 50 cells. To this end, we seeded HaCat, A-375, or B16-F10 cells and exposed them to different **Ru4** concentrations for 24 h. After this period, we added fresh culture medium without **Ru4** to the plates and maintained them in the incubator for 10 days. This allowed us to evaluate how **Ru4** affects colony formation, size, and number.

According to Fig. 6, **Ru4** reduced the number of colonies in a concentration-dependent manner. Additionally, HaCat cells formed a larger number of colonies than A-375 and B16-F10 cells. This agreed with the selectivity observed in the cytotoxic activity revealed by the XTT assay. Thus, **Ru4** exhibited cytostatic effects, which prevent cell growth, development, and multiplication. **Ru4** was also cytotoxic because, depending on the concentration, it completely inhibited cell growth. This behavior is similar than observed for cisplatin in A-375 cancer cells.[42]

Moreover, we investigated how **Ru4** affects A-375 cell morphology. For this purpose, we treated A-375 cells with different **Ru4** concentrations and captured images immediately after treatment and after treatment for 24 h (Fig. 7). After treatment for 24 h, A-375 cells presented morphological alterations, especially at 5, 10, and 20 μM **Ru4** A-375 cells lost adhesion and were less dense. In addition, dead cells became more evident compared to the control (1% DMSO).

Cell migration is a fundamental process during the natural development of an organism and is important for wound healing, tissue repair and development, and defense. However,

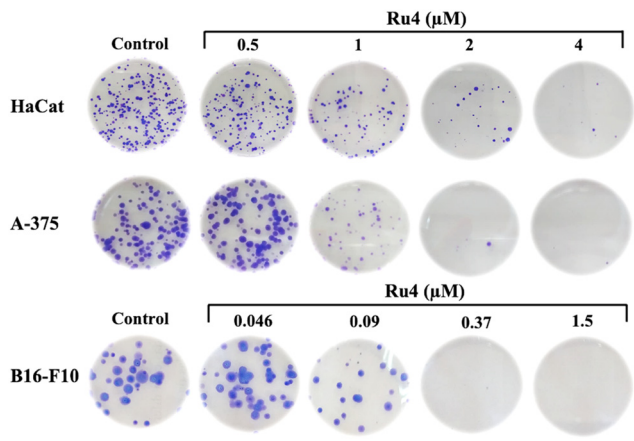


Fig. 6 Representative images obtained during the clonogenic assay demonstrating how the **Ru4** complex affects colony formation by HaCat, A-375, and B16-F10 cells.

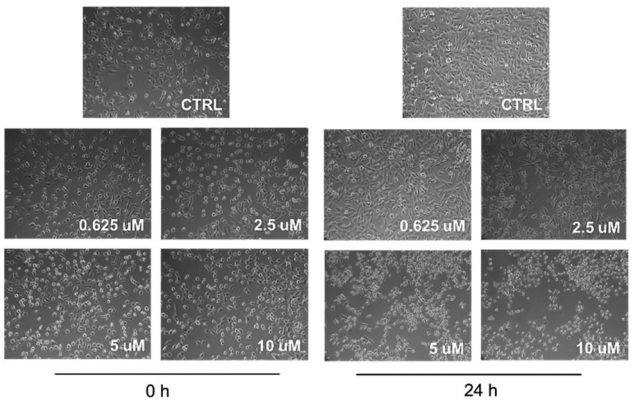


Fig. 7 Effect of different concentrations of the **Ru4** complex on the morphology of human melanoma cells, A-375, immediately after treatment and after treatment for 24 h. 10 × magnification of the objective.

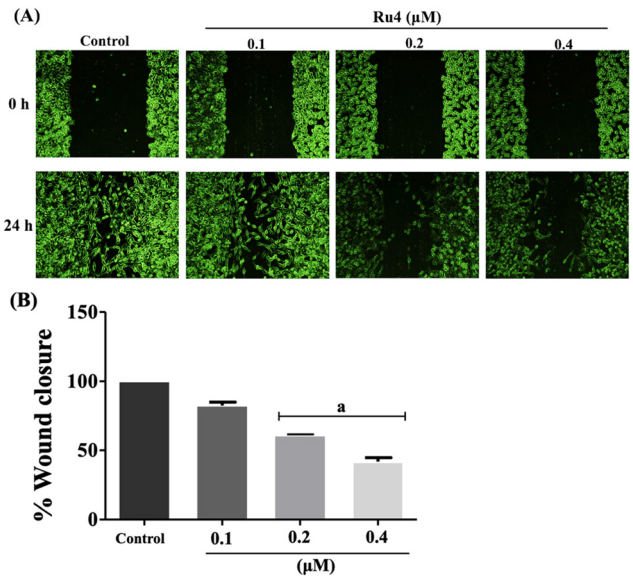


Fig. 8 (A) Representative images of A-375 cells after treatment with the **Ru4** complex for 24 h, captured with an inverted microscope (4×). (B) Quantitative assessment of cell migration following treatment with the **Ru4** complex, conducted by measuring the extent of cell wound closure with the Image J software.

cell migration can contribute to the appearance of metastases, when a tumor cell migrates from a primary tumor to another region of the body, where it undergoes adhesion processes and gives rise to a new tumor. Therefore, a compound that inhibits cell migration is key for directly inhibiting or controlling metastasis.[43,44]

In this sense, we investigated whether **Ru4** inhibits cell migration. To this end, we seeded A-375 cells, and, after they reached confluence, we made a scratch on the adherent cell monolayer with sterile pipette tip. We added culture medium containing different **Ru4** concentrations to the cells and captured images of the scratch immediately after we added **Ru4** and after treatment for 24 h. Fig. 8 shows that 0.2 and 0.4 μM **Ru4** inhibited cell migration given that the wound was not completely closed compared to the control (1% DMSO). Hence, **Ru4** could potentially inhibit cell migration.

## Conclusions

We synthesized and characterized five ruthenium complexes. Four of the ruthenium complexes (**Ru1–Ru4**) contained two diphosphines and one 2-mercapto-4(3*H*)-quinazoline as ligands, whereas one ruthenium complex (**Ru5**) contained two bipyridines and one 2-mercapto-4(3*H*)-quinazoline as ligands. In addition, we investigated the cytotoxic activities of **Ru2–Ru5** against melanoma cell lines. All the complexes inhibited melanoma cell growth (B16-F10 and A-375 cells) in a dose-dependent manner. **Ru4**, bearing two dppen, exhibited four times greater activity against A-375 tumor cells compared to non-tumor HaCat cells. Additionally, **Ru4** inhibited colony formation in both HaCat and A-375 cells (with a more pronounced effect on the latter cells), altered A-375 cell morphology, and inhibited cell migration at concentrations of 0.2 and 0.4 μM. Furthermore, we evaluated the ability of the ruthenium complexes to interact with biomolecules such as DNA and HSA by various analytical techniques. The ruthenium complexes interacted with DNA weakly, possibly through the grooves, and they interacted with HSA moderately. The ruthenium complexes bearing phosphine and mercapto as ligands displayed promising cytotoxic properties against melanoma. Our results confirmed our previous data on the cytotoxic activity of ruthenium complexes containing phosphines as ligands, which were even better than similar complexes containing bipyridine ligands.[40]

## Author contributions

Nádija N. P. da Silva: writing – original draft, validation, methodology, investigation, formal analysis, data curation, conceptualization. Marcos V. Palmeira-Mello: writing – original draft, methodology, formal analysis, data curation. Nathália O. Acésio: methodology, formal analysis, data curation. Carlos A. F. Moraes: methodology, formal analysis, data curation. João Honorato: methodology, formal analysis, data curation. Eduardo E. Castellano: methodology, formal analysis, data curation. Denise C. Tavares: methodology, formal analysis, data curation. Katia M. Oliveira: writing – original draft, validation, methodology, investigation. Alzir A. Batista: writing – review and editing, writing original draft, visualization, validation, supervision, funding acquisition, formal analysis, conceptualization.

## Data availability

The data supporting this article have been included as part of the ESI.†

Crystallographic data for **Ru1**, **Ru2** and **Ru5** has been deposited at the CCDC 2355448 (**Ru1**), 2355449 (**Ru2**) and 2355450 (**Ru5**).†

## Conflicts of interest

There are no conflicts to declare.

## Acknowledgements

The authors are grateful for the financial support of the Brazilian Research Agencies CAPES, CNPq, FAPESP, and FAPDF. K. M. Oliveira would like to thank Fundação de Apoio à Pesquisa do Distrito Federal (FAPDF, process 00193-00002088/2023-42) and Decanatos de Pesquisa e Inovação e da Pós-graduação (DPI/DPG) da Universidade de Brasília (UnB) for the financial support provided. N. N. P. da Silva thanks Conselho Nacional de Desenvolvimento Científico e Tecnológico (CNPq, process 130556/2021-1) for financial support. M. V. Palmeira-Mello thanks Fundação de Apoio à Pesquisa do Estado de São Paulo (FAPESP, process 2021/01787-0). Alzir A. Batista thanks FAPESP for financial support (Processes 2023/02475-8 and 2017/15850-0).

## References

1 Q. Lin, X. Guo, B. Feng, J. Guo, S. Ni and H. Dong, *Comput. Biol. Med.*, 2024, 108549.
2 S. Carr, C. Smith and J. Wernberg, *Surg. Clin. North Am.*, 2020, **100**, 1–12.
3 C. Liang, P. Wang, M. Li, R. Li, K. P. Lai and J. Chen, *Heliyon*, 2024, **10**, e28616.
4 C. M. Manzano, D. H. Nakahata and R. E. F. de Paiva, *Coord. Chem. Rev.*, 2022, **462**, 214506.
5 B. L. V. Rosenberg, *Nature*, 1969, **224**, 488–490.
6 K. D. Mjos and C. Orvig, *Chem. Rev.*, 2014, **114**, 4540–4563.
7 Q. Peña, A. Wang, O. Zaremba, Y. Shi, H. W. Scheeren, J. M. Metselaar, F. Kiessling, R. M. Pallares, S. Wuttke and T. Lammers, *Chem. Soc. Rev.*, 2022, **51**, 2544–2582.
8 L. Zeng, P. Gupta, Y. Chen, E. Wang, L. Ji, H. Chao and Z.-S. Chen, *Chem. Soc. Rev.*, 2017, **46**, 5771–5804.
9 I. Yousuf, M. Bashir, F. Arjmand and S. Tabassum, *Coord. Chem. Rev.*, 2021, **445**, 214104.

10 A. Casini and A. Pöthig, *ACS Cent. Sci.*, 2024, **10**, 242–250.
11 X. Xiong, L.-Y. Liu, Z.-W. Mao and T. Zou, *Coord. Chem. Rev.*, 2022, **453**, 214311.
12 S. Thota, D. A. Rodrigues, D. C. Crans and E. J. Barreiro, *J. Med. Chem.*, 2018, **61**, 5805–5821.
13 S. Monro, K. L. Colón, H. Yin, J. Roque, P. Konda, S. Gujar, R. P. Thummel, L. Lilge, C. G. Cameron and S. A. McFarland, *Chem. Rev.*, 2019, **119**, 797–828.
14 C. Sumithaa and M. Ganeshpandian, *Mol. Pharm.*, 2023, **20**, 1453–1479.
15 S. M. Meier-Menches, C. Gerner, W. Berger, C. G. Hartinger and B. K. Keppler, *Chem. Soc. Rev.*, 2018, **47**, 909–928.
16 G. F. Grawe, K. M. Oliveira, C. M. Leite, T. D. de Oliveira, J. Honorato, A. G. Ferreira, E. E. Castellano, M. R. Cominetti, R. S. Correa and A. A. Batista, *Dalton Trans.*, 2022, **51**, 1489–1501.
17 A. E. Graminha, C. Popolin, J. Honorato, R. S. Correa, K. M. de Oliveira, L. R. Godoy, L. C. Vegas, J. Ellena, A. A. Batista and M. R. Cominetti, *Eur. J. Med. Chem.*, 2022, **243**, 114772.
18 G. F. Grawe, K. M. Oliveira, C. M. Leite, T. D. de Oliveira, A. R. Costa, C. A. F. Moraes, J. Honorato, M. R. Cominetti, E. E. Castellano, R. S. Correa, S. P. Machado and A. A. Batista, *J. Inorg. Biochem.*, 2023, **244**, 112204.
19 M. M. da Silva, G. H. Ribeiro, M. S. de Camargo, A. G. Ferreira, L. Ribeiro, M. I. F. Barbosa, V. M. Deflon, S. Castelli, A. Desideri, R. S. Corrêa, A. B. Ribeiro, H. D. Nicolella, S. D. Ozelin, D. C. Tavares and A. A. Batista, *Inorg. Chem.*, 2021, **60**, 14174–14189.
20 M. V. Palmeira-Mello, A. R. Costa, L. P. de Oliveira, O. Blacque, G. Gasser and A. A. Batista, *Dalton Trans.*, 2024, **53**, 10947–10960.
21 A. A. Batista, L. A. C. Cordeiro, G. Oliva and O. R. Nascimento, *Inorg. Chim. Acta*, 1997, **258**, 131–137.
22 B. P. Sullivan, D. J. Salmon and T. J. Meyer, *Inorg. Chem.*, 1978, **17**, 3334–3341.
23 M. T. Bautista, E. P. Cappellani, S. D. Drouin, R. H. Morris, C. T. Schweitzer, A. Sella and J. Zubkowski, *J. Am. Chem. Soc.*, 1991, **113**, 4876–4887.
24 B. P. Sullivan and T. J. Meyer, *Inorg. Chem.*, 1982, **21**, 1037–1040.
25 G. M. Sheldrick, *Acta Crystallogr., Sect. C: Struct. Chem.*, 2015, **71**, 3–8.
26 O. V. Dolomanov, L. J. Bourhis, R. J. Gildea, J. A. K. Howard and H. Puschmann, *J. Appl. Crystallogr.*, 2009, **42**, 339–341.
27 J. R. Lacowicz, *Principles of Fluorescence Spectroscopy*, Kluver Academic/Plenum Publishers, New York, 1999.
28 M. Ganeshpandian, R. Loganathan, E. Suresh, A. Riyasdeen, M. A. Akbarsha and M. Palaniandavar, *Dalton Trans.*, 2014, **43**, 1203–1219.
29 N. A. P. Franken, H. M. Rodermond, J. Stap, J. Haveman and C. van Bree, *Nat. Protoc.*, 2006, **1**, 2315–2319.
30 K. Nakamoto, *Infrared and Raman spectra of inorganic and coordination compounds*, New York, 4th edn, 2009.
31 G. H. Ribeiro, A. P. M. Guedes, T. D. De Oliveira, C. R. S. T. b. De Correia, L. Colina-Vegas, M. A. Lima, J. A. Nóbrega, M. R. Cominetti, F. V. Rocha, A. G. Ferreira, E. E. Castellano, F. R. Teixeira and A. A. Batista, *Inorg. Chem.*, 2020, **59**, 15004–15018.
32 K. M. Oliveira, J. Honorato, F. C. Demidoff, M. S. Schultz, C. D. Netto, M. R. Cominetti, R. S. Correa and A. A. Batista, *J. Inorg. Biochem.*, 2021, **214**, 111289.
33 A. Kellett, Z. Molphy, C. Slator, V. McKee and N. P. Farrell, *Chem. Soc. Rev.*, 2019, **48**, 971–988.
34 T. Biver, F. Secco and M. Venturini, *Coord. Chem. Rev.*, 2008, **252**, 1163–1177.
35 Y. Wei and L.-H. Guo, *Environ. Toxicol. Chem.*, 2009, **28**, 940–945.
36 S. U. Rehman, T. Sarwar, M. A. Husain, H. M. Ishqi and M. Tabish, *Arch. Biochem. Biophys.*, 2015, **576**, 49–60.
37 M. V. Palmeira-Mello, A. B. Caballero, P. Herrera-Ramírez, A. R. Costa, S. S. Santana, G. P. Guedes, A. Caubet, A. A. Batista, P. Gamez and M. Lanznaster, *J. Inorg. Biochem.*, 2023, **248**, 112345.
38 B. N. Cunha, L. Colina-Vegas, A. M. Plutín, R. G. Silveira, J. Honorato, K. M. Oliveira, M. R. Cominetti, A. G. Ferreira, E. E. Castellano and A. A. Batista, *J. Inorg. Biochem.*, 2018, **186**, 147–156.
39 P. D. Ross and S. Subramanian, *Biochemistry*, 1981, **20**, 3096–3102.
40 R. A. De Grandis, P. W. da S. dos Santos, K. M. de Oliveira, A. R. T. Machado, A. F. Aissa, A. A. Batista, L. M. G. Antunes and F. R. Pavan, *Bioorg. Chem.*, 2019, **85**, 455–468.
41 A. P. Carnizello, M. I. F. Barbosa, M. Martins, N. H. Ferreira, P. F. Oliveira, G. M. Magalhães, A. A. Batista and D. C. Tavares, *J. Inorg. Biochem.*, 2016, **164**, 42–48.
42 G. C. Segat, C. G. Moreira, E. C. Santos, M. Heller, R. C. Schwanke, A. V. Aksenov, N. A. Aksenov, D. A. Aksenov, A. Kornienko, R. Marcon and J. B. Calixto, *Invest. New Drugs*, 2020, **38**, 977–989.
43 S. A. Eccles and D. R. Welch, *Lancet*, 2007, **369**, 1742–1757.
44 H. Yamaguchi, J. Wyckoff and J. Condeelis, *Curr. Opin. Cell Biol.*, 2005, **17**, 559–564.